

COVER CRACKING OF THE REINFORCED CONCRETE DUE TO REBAR CORROSION INDUCED BY CHLORIDE PENETRATION

JAIME C. GÁLVEZ^{*}, SANTIAGO GUZMÁN^{*} AND JOSÉ M. SANCHO[†]

^{*} E.T.S. Ingenieros Caminos, Canales y Puertos. Universidad Politécnica Madrid.
C/ Profesor Aranguren s/n, 28040 Madrid, Spain.
e-mail: jaime.galvez@upm.es; guzman.s@trsa.es

[†] E.T.S. Arquitectura. Universidad Politécnica Madrid.
Av. Juan de Herrera s/n, 28040 Madrid, Spain.
e-mail: jose.sancho@upm.es

Key words: Concrete, Cracking, Corrosion, Chloride, Durability, Diffusion.

Abstract: This paper is focused on the problem of the chloride-induced corrosion of the rebar in reinforced concrete, particularly in the case of slabs and decks of bridges. A comprehensive model for the chloride ingress into concrete is presented, with special attention to non-linear diffusion coefficients, chloride binding isotherms and convection phenomena. The model tries to use a priori parameter estimations, according to material characteristics and external environment conditions, instead of a posteriori best fit. Complex geometries, like random cracks, can also be incorporated. Based on the results of chloride diffusion, subsequent active corrosion is assumed and the radial expansion of the corroded reinforcement reproduced. For cracking simulation, the Strong Discontinuity Approach is applied. Both models, corresponding to initiation and propagation corrosion stages, are incorporated in the same finite element program and chained. Comparisons with experimental results are carried out, with reasonably good agreements being obtained, especially for cracking patterns. Major limitations refer to difficulties to establish precise levels of basic data such as the chloride ion content at concrete surface, the chloride threshold concentration that triggers active corrosion, the rate of oxide production or the rust mechanical properties.

1 INTRODUCTION

Cracking of concrete cover due to corrosion-induced expansion of steel rebar is one of the major causes of the deterioration of reinforced concrete (RC) structures exposed to marine environments and de-icing salts which may lead to failure and even collapse. In any case, the cost of associated repair and maintenance is enormous [1].

Yet despite massive research effort related to the concrete durability in recent years, many factors involved in the chloride-induced corrosion process remain poorly understood. In spite of significant progress in predicting models, the estimation of service life of RC

structures is to be more fully and satisfactorily defined.

This work presents two models that deal with the chloride-induced corrosion in RC structures corresponding to the two distinct phases traditionally adopted in the literature [2]. The former (initiation stage) analyses the chloride diffusion within partially saturated concrete. A comprehensive model is developed through the governing equations of moisture, heat and chloride-ion flow. The latter (propagation stage) describes the internal cracking around the bar due to expansive pressures as corrosion of the reinforcing bar progresses, once a certain chloride

concentration threshold is reached.

This paper presents a meso-modelling procedure for analysis of the chloride ingress and transportation and concrete cracking. Both models are incorporated in a Finite Element (FE) code and comparisons with experimental data show a reasonably good agreement. The ultimate objective of this work is to try to integrate the two traditional phases (initiation and propagation) based on Tuutti's conceptual model, widely used in the literature and usually analysed separately. The estimation of the service life of the structure needs to evaluate the associated time for each one.

With reference to the initiation stage, though the former approaches considered the transport of ions only under the effect of diffusion by the mere application of 2nd Fick's law, other phenomena such as convection (motion of dissolved substances caused by flow of water in pore solution of partially saturated media) or chloride binding (capacity of free chloride of being chemically bound) are soon taken into account. Here a self-programmed computer code is implemented. Given the ideal nature of the ionic solutions, activity effects can be neglected. Likewise, the effect of chloride binding is introduced under local chemical equilibrium, valid except for cases where ions are transported very quickly through the material pore structure, e.g., under an externally applied electrical potential. Conventionally, chloride binding is taken into account in the diffusion process by means of an apparent diffusion coefficient [3,4]. Instead, the present approach develops the complete set of time-dependent equations for both the chloride concentration within the pore solution (through an intrinsic effective diffusion coefficient) and the moisture content within the pore space [5,6], by averaging the relevant microscopic transport equations over a representative volume element. Three macroscopic variables are used: chloride concentration, moisture and temperature.

The present approach focuses attention on the interdependence between chloride and moisture flows, with variable diffusion coefficients [3,7]. Influence of temperature, hydration time, chloride binding or

hygrometric condition is clearly marked. The proposed FE model reproduces results of experimental tests by means of a priori parameter estimation, according to the characteristics of materials (e.g., porosity, ratio w/c or compressive strength) and external environment conditions. The model can also reproduce bi-dimensional complex geometries; e.g. cracked concrete cover where transport of both ions and moisture within the crack is also considered (Figure 1). However, basic variables such as surface chloride content or threshold chloride concentration are supposed to be known though, in fact, they are not precisely defined in most practical cases.

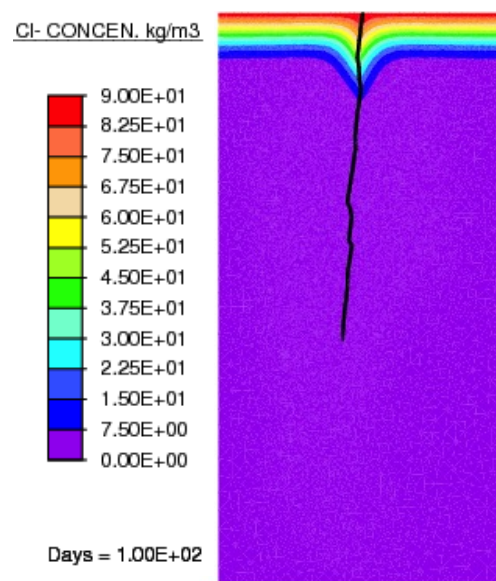


Figure 1: Influence of a surface crack in chloride profile.

Regarding propagation stage, corrosion provokes the reinforcement cross-section reduction and loss of bond between concrete and steel. Moreover, oxide products occupy much greater volume than the original steel consumed. Tensile stresses are generated in the surrounding concrete, resulting in cracking and, eventually, spalling and delamination. Analytical implementation of the discrete crack model, based on the thick walled-cylinder approach and FE implementation of the smeared crack approach has been widely used to simulate this stage ([8-10], among others). However, the thick walled-cylinder approach introduces some difficulties when

extended to real and practical cases, with complex geometry. Likewise, the smeared crack approach may lead to an ill-posed system of equations, localisation instabilities and spurious mesh sensitivity of the FE calculations [11]. More recently, the so-called Strong Discontinuity Approach (SDA) has been applied. In this approach, the fracture zone is represented as a discontinuous displacement surface but not restricted to inter-element lines, because the displacements jumps are embedded in the corresponding finite element formulation.

This work presents a procedure, based on the SDA, which reproduces the fracture process of concrete by means of an embedded cohesive crack finite element [12,13]. The model has been successful when applied to the fracture of concrete and only requires standard properties of the material, measured by standardised methods. Once some conceptual difficulties concerning the localisation of cracks are solved, the proposed model is capable to estimate time to surface cracking quite accurately; although it is necessary to make some assumptions about the consideration of a special porous zone around the steel-concrete interface and the accommodation of corrosion products within the open cracks generated in the process.

2 THE INITIATION STAGE

There are four basic mechanisms concerning the movement of ions and fluids through concrete pores, namely: capillary suction, due to surface tension acting in capillaries of cement paste; permeation, related to pressure gradients; diffusion, corresponding to concentration gradients; and migration, due to electrical potential gradients.

As a first approach to the problem, neglecting the transference of electric charges and the state of stress of the material, two basic mechanisms govern the transport of ions into unsaturated concrete: diffusion and capillary suction (convection).

In such a way, equations used to reproduce chloride transport in concrete are based on three fundamental variables: chloride

concentration C_c (kg/m³), evaporable water content ω_e and temperature T .

With respect to the first variable, differences between the concentration of bound chlorides C_{bc} (kg/m³ of concrete) and the free chloride concentration C_{fc} (kg/m³ of pore solution) must be distinguished. The total chloride concentration C_{tc} (kg/m³ of concrete) then provides [3]:

$$C_{tc} = C_{bc} + \omega_e C_{fc} \quad (1)$$

2.1 Diffusion

Chloride diffusion in unsaturated concrete is rather complicated and differs notably from that described by Fick's law.

However, from a practical point of view, the use of Fick's law in a generalised way is accepted in the literature, defining an effective value of diffusion coefficient D_c or diffusivity:

$$\mathbf{J}_d = -\omega_e D_c \nabla C_{fc} \quad (2)$$

where \mathbf{J}_d refers to diffusion flux of chloride in concrete per unit area and per unit time (kg/m²/s) and D_c (m²/s) is the effective diffusion coefficient that depends, at least, on concentration, humidity and temperature [3,7].

2.2 Capillary suction

Models describing moisture diffusion in concrete are usually based on an extension of Darcy's law as a constitutive equation. Nevertheless, phenomena of water diffusion in concrete are highly non-linear. An apparent diffusivity D_h , that takes into account humidity, temperature and, also, equivalent hydration time, is used again. In addition, the equation is not formulated in terms of water content ω_e , but relative humidity h .

Water is first adsorbed on the surface of capillary pores and, then, water condensates as the relative humidity increases. Under equilibrium conditions, the pore relative humidity and evaporable water content can be related by sorption and desorption isotherms [7].

Although the described water transport is due to the capillary potential gradient and consequently not, strictly, a diffusion process,

through mass conservation and assuming no chemical reaction between water and solid phase and a constant solution density, the following relationship arises:

$$\frac{\partial \omega_e}{\partial t} = \text{div}(D_h \nabla h) \quad (3)$$

Likewise, the vaporisation ratio per unit volume in the liquid/gas interface should be considered [6], though here it has been neglected for the sake of simplicity.

2.3 Heat transfer

Temperature is the third basic variable of the system of equations defined below. Heat transfer is described by means of the first law of thermodynamics, an expression of the principle of conservation of energy, and Fourier's law, with the following well-known equation (in the case of neither heat sources nor soaks):

$$\frac{\partial}{\partial t}(\rho c T) = \text{div}(\lambda \nabla T) \quad (4)$$

where ρ is the material density, c is the specific heat and λ the thermal conductivity. Adopting constant values for these three parameters, the resulting equation is linear. Non-linearity of problems related to humidity and chloride concentration comes from the dependence of diffusion coefficients on the abovementioned variables. Even considering a linear heat transfer equation, decoupled then from the previous equations corresponding to chloride concentration and moisture diffusion, it is worth noting that the different coefficients involved in the system of equations are, in general, highly dependent on temperature.

2.4 Chloride ion transport

On the basis shown in the previous paragraphs, the total free chloride flux in concrete \mathbf{J}_{fc} (kg/m²/s) can be obtained by the addition of the flux due to chloride concentration diffusion and the flux due to convection, i.e., ion transport driven by flux of moisture through concrete:

$$\mathbf{J}_{fc} = -\omega_e D_c \nabla C_{fc} - C_{fc} D_h \nabla h \quad (5)$$

Through the mass balance of solute:

$$\frac{\partial C_{tc}}{\partial t} = -\text{div}(\mathbf{J}_{fc}) \quad (6)$$

The following expression is obtained:

$$\left(\frac{\partial C_{bc}}{\partial C_{fc}} + \omega_e \right) \frac{\partial C_{fc}}{\partial t} + C_{fc} \frac{\partial \omega_e}{\partial t} = \text{div}(C_{fc} D_h \nabla h) + \text{div}(\omega_e D_c \nabla C_{fc}) \quad (7)$$

Although chloride binding is not an instantaneous process and one which involves more factors such as the pH of the solution, in practice the models from literature use binding isotherm curves (see Figure 2) in assuming an instantaneous and completely reversible equilibrium between free and bound chlorides.

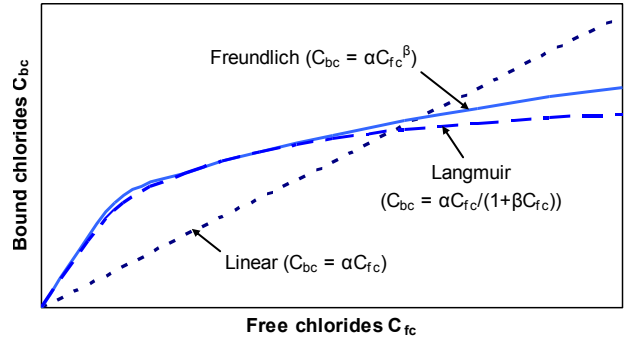


Figure 2: Chloride binding isotherm curves.

2.5 Finite element formulation

The mentioned analysis leads to a system of three partial differential equations with three variables: free chloride concentration C_{fc} , relative humidity h and temperature T . Moreover, values of C_{bc} (bound chlorides) and ω_e (pore water content) must be known as a function of C_{fc} and h , respectively.

Developing the chloride transport case, equation (7) can be expressed in matrix notation, into elemental cells Ω_e , through nodal shape functions N_I :

$$c_{c(e)} \cdot C_{fc}^{(e)} + k_{c(e)} C_{fc}^{(e)} + f_{c(e)} = 0 \quad (8)$$

The non-linearity of the problem arises from the dependence of capacitance matrix c_c and stiffness matrix k_c on the unknown variables: concentration, humidity and

temperature.

For the capacitance matrix, the following arises:

$$c_{c(e)}^{IJ} = \int_{\Omega_e} N_I \left(\frac{\partial C_{bc}}{\partial C_{fc}} + \omega_e \right) N_J d\Omega_e \quad (9)$$

With respect to the system stiffness matrix:

$$k_{c(e)}^{IJ} = \int_{\Omega_e} \nabla N_I (\omega_e D_c) \nabla N_J d\Omega_e - \int_{\Omega_e} N_I (D_h \nabla h) \nabla N_J d\Omega_e \quad (10)$$

Finally, the vector of equivalent nodal forces is given by:

$$f_{c(e)}^I = \oint_{\partial\Omega_e} N_I (\mathbf{J}_d)_n d\Gamma_e \quad (11)$$

This vector is considered especially in those elements at borders where the diffusion flux \mathbf{J}_d is known.

In a similar way, humidity and temperature cases can be developed.

Here, the element matrices and vectors needed to assemble the non-linear equations were programmed in a user subroutine in the framework of the Finite Element Analysis Program (FEAP), developed by Taylor [14]. The reader is referred to [15] for a more detailed description of the analyses.

2.6 Model contrast

In order to verify the proposed model, an experimental study carried out by Sergi et al. [16] is simulated. A cylindrical hardened specimen was submerged in a 1M NaCl solution for 100 days, with all surfaces isolated except the top free. The problem to be analysed is then a sudden increase in Cl⁻ concentration in the top surface of the concrete sample, accompanied by a change in the ambient relative humidity, under the hypothesis that this sudden increase in the free surface remains constant over time. In the other boundary model edges, a null flux condition is imposed.

The first approximation is based on a simple model through Fick's second law that has an analytical solution for the one-dimensional case of a semi-infinite medium

with constant diffusion coefficients:

$$C(x,t) = C_s - (C_s - C_i) \cdot \left[\operatorname{erf} \left(\frac{x}{\sqrt{4Dt}} \right) \right] \quad (12)$$

where C represents the chloride concentration, C_s is the surface concentration, C_i the initial value, D is the diffusion coefficient (constant), t the time and x the distance to the free surface.

This simple model takes everything into account by modifying the chloride diffusion coefficient in order to achieve the best fit. This is the reason for the apparent diffusion coefficient of concrete varying from 10^{-10} to 10^{-12} m²/s in the literature [17].

Here the described comprehensive model will be used, taking into account separately aspects such as chloride binding or relative humidity changes and employing an estimation a priori of the diffusion coefficient.

According to [3], D_c is varying with temperature, humidity and equivalent hydration time:

$$D_c = D_{c,ref} F_1(T) F_2(t_e) F_3(h) \quad (13)$$

Similarly, regarding humidity transport:

$$D_h = D_{h,ref} G_2(T) G_1(h) G_3(t_e) \quad (14)$$

Figure 3 reproduces the free chloride concentration profile at 100 days. Firstly, experimental data are presented. Secondly, the results by the best fit to Fick's equation, with results to an apparent diffusion coefficient of 1.35×10^{-11} m²/s. Better results are obtained by considering the binding effect through Freundlich isotherm ($\alpha_F = 0.88$; $\beta_F = 0.47$). In this case, the apparent diffusion coefficient is equal to 4.28×10^{-11} m²/s but, again, the analysis a posteriori of experimental data appears indispensable.

However, in the present model, an intrinsic diffusion coefficient proposed by Wang et al. [17] that equals 1.02×10^{-10} m²/s divided by a tortuosity factor ($\tau = 1.9$) squared is used, i.e. 2.825×10^{-11} m²/s. The influence of convection is clearly shown by comparing results obtained by considering the initial humidity of 80% in the samples of the test to those considering a saturated condition from the very beginning. For humidity transport, a

linear relation between water content and humidity was assumed and average parameters from literature adopted for parameters affecting D_h .

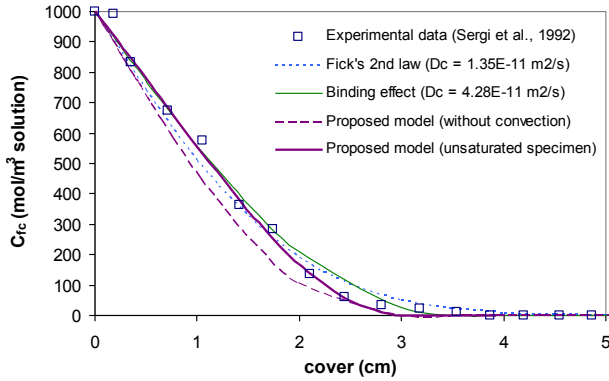


Figure 3: Free chloride profile after 100 days (please refer to tests by Sergi et al. [16]).

Regarding the total chloride profile, a good fit with experimental data is obtained. No information is obtained through simple models based exclusively on the second Fick's law.

3 THE PROPAGATION STAGE

Once the chloride concentration threshold has been reached in the rebar surroundings, the subsequent oxide generation increases the total equivalent rebar section. The volume of the rust products is about four- to six-times higher than that of steel. Consequently, expansive stress appears in the concrete, causing cracking of the cover (see Figure 4).

In spite of the variety of the proposed models [8-10,18-22], most are based on the hypothesis of a thick-walled cylinder with the wall thickness equal to that of the concrete cover, with different approaches to the non-linear behaviour of concrete after cracking.

Here, a finite element with a cohesive embedded crack will be used [23]. Once again, a FEAP program is employed. In fact, the same meshes as used in initiation stage models are appropriate for the propagation stage, as a first step in completing integration of the two phases.

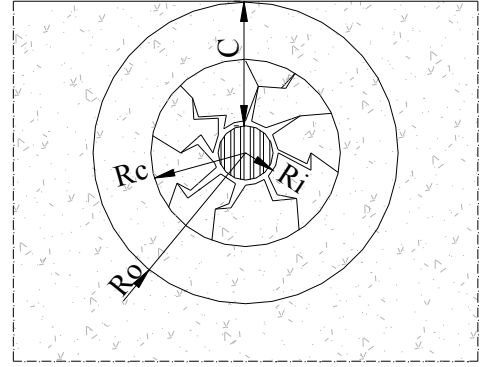


Figure 4: Sketch of cover cracking due to expansion of rebar corrosion products.

This embedded crack element does not need a crack tracking algorithm. As the cracking pattern caused by corrosion phenomena includes multiple cracks and branching, this feature of the used formulation is of special relevance. The plane model avoids the classical central symmetry condition with respect to the bar axis with a contact algorithm employed to reproduce the oxide-concrete interface.

3.1 Finite element with cohesive embedded crack

A simple generalisation of the cohesive crack to mixed mode is used, one which assumes that the traction vector \mathbf{t} transmitted across the crack faces is parallel to the crack displacement vector \mathbf{w} (central forces model). To cope with the possibility of unloading [12,13]:

$$\mathbf{t} = \frac{f(\tilde{w})}{\tilde{w}} \mathbf{w} \quad (15)$$

where $f(\tilde{w})$ is the classical softening function for pure opening mode (Figure 5) and \tilde{w} is an equivalent crack opening defined as the historical maximum of the magnitude of the crack displacement vector.

The process is as follows. Within each element, initially, $\mathbf{w} = \mathbf{0}$ and linear elastic behaviour is assumed. If maximum principal stress exceeds the tensile strength, then a crack appears perpendicular to the corresponding direction and \mathbf{n} is computed as a unit

eigenvector of $\boldsymbol{\sigma} = \mathbf{E}:\boldsymbol{\varepsilon}^a$, where $\boldsymbol{\varepsilon}^a$ is the apparent strain tensor. Limiting the analysis to CST elements, a node is selected so that the side opposite to it is as parallel as possible to the crack [12,13,24]. Then, vector \mathbf{b}^+ can be determined as the unit vector orthogonal to this opposite side.

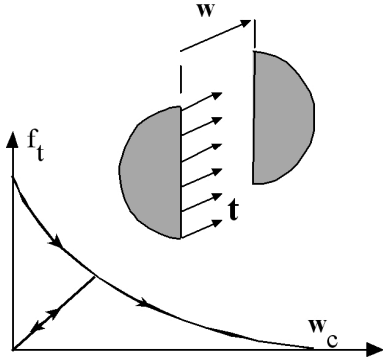


Figure 5: Sketch of softening curve for the cohesive crack model.

Developing the expressions from the strong discontinuity approach [12,13,23]:

$$\left[\frac{f(\tilde{w})}{\tilde{w}} \mathbf{1} + \mathbf{n} \cdot \mathbf{E} \cdot \mathbf{b}^+ \right] \cdot \mathbf{w} = [\mathbf{E}:\boldsymbol{\varepsilon}^a] \cdot \mathbf{n} \quad (16)$$

This equation is solved for \mathbf{w} using the Newton-Raphson method given the nodal displacements (and so $\boldsymbol{\varepsilon}^a$) once the crack is formed and thus \mathbf{n} and \mathbf{b}^+ are also known.

To avoid locking after a certain crack growth, the opportunity of crack adaptability within each element is provided, allowing the crack to adapt itself to the later variations in principal stress direction while its opening is small. The threshold value must be related to the softening properties of the material. Having exceeded these threshold values, the crack is considered consolidated and the crack direction becomes fixed.

3.2 Model contrast

Once again, the numerical model should be contrasted with experimental results. On this occasion, the reference is the slab specimen L1 subjected to accelerated corrosion tests developed by Liu [25]. Table 1 summarises the main experimental data.

Table 1: Experimental data of slab specimen L1 [26]

Parameter	Symbol	Value	Unit
Initial rebar diameter	D_i	16	mm
Clear cover to the reinforcement	c	48	mm
Rebar spacing	s	200	mm
Annual mean corrosion rate	i_{cor}	2.41	$\mu\text{A}/\text{cm}^2$
Concrete strength	f_c	31.5	MPa
Concrete elasticity modulus	E_c	27.0	GPa
Tensile concrete strength	f_{ct}	3.3	MPa
Concrete Poisson ratio	ν_c	0.18	-
Creep coefficient	ϕ	2.0	-
Porous zone around steel-concr. interface	d_o	12.5	μm

For the sake of simplicity, the mechanical properties of oxide products are adopted as the steel ones, in accordance with the assumption offered by Bhargava and Ghosh [9]. A contact element in the steel (oxide)-concrete interface is necessary to localise cracking and avoid tensile stress in the reinforcement bar. A perfect sliding contact was chosen here. Additionally, a porous zone (in fact, an especially porous zone) around the bar is considered, taking into account that corrosion products accumulating around the reinforcement bar do not exert any pressure on the surrounding concrete until they fully fill voids between steel and concrete.

Oxide production is modelled as an increment of area in the rebar section, as usually adopted in the literature. The initial radius of steel bar R_i is reduced to R_i^* , while corrosion products would reach a radius $R_i + \Delta$ if not constrained by concrete. Uniform corrosion around the bar is then assumed. In addition, the plane strain condition is considered, as well as the exponential function for a softening curve with an estimated value of $G_F = 100$ N/m.

Loss of steel mass j_s is related to the amount of current i_{cor} using Faraday's law:

$$j_s = \frac{M_{Fe} i_{cor}}{nF} \quad (17)$$

where M_{FE} is the atomic weight of iron (55.9

g/mol), n the valence of the reaction (typically, $n = 2$ or 3) and F the Faraday's constant.

Through knowing the ratio of molecular weight of iron to the molecular weight of the corrosion products μ_w , the density of rust can be evaluated through the following expression:

$$\rho_r = \frac{\rho_s}{\mu_w \mu_v} \quad (18)$$

where μ_v defines the ratio of volume of expansive corrosion products to the volume of steel consumed.

If i_{cor} is assumed constant (not always applicable, especially in a highly varying aggressive environment [4]), the rate of the loss of steel mass j_s and, consequently through μ_w parameter, the rate of rust production is constant. However, some authors (e.g., [8]) consider that the rate of rust production is not unchanging but inversely proportional to the amount of corrosion products, i.e., decreasing with time. These models are based on a time-invariant parameter k_p used to fit experimental data, but differing by more than one order of magnitude among the proposed values in the literature. In this analysis, the rate of rust production is set constant and expressed by means of the Faraday's law, in order not to underestimate the rate of steel loss caused by corrosion [26].

Specifically, $\mu_w = 0.613$ and $\mu_v = 3.39$ [21] were assumed. For a steel density of $7,860 \text{ kg/m}^3$, rust density equals to $3,780 \text{ kg/m}^3$. The time t is related to radius increment Δ through the expression:

$$t(\Delta) = \frac{\rho_s}{4D_i j_s (\mu_v - 1)} \left[(D_i + 2\Delta)^2 - D_i^2 \right] \quad (19)$$

Additionally, an increment in time to cracking around 90 days is due to the fill of porous zone around the rebar as previously commented.

Estimation of time to cracking is slightly lower than the experimental ones (1.84 years [25]). However, if amount of corrosion products that has been accommodated within the open cracks during the progress of cracking is taken into account, experimental values are tallied. Likewise, major limitations

refer to the quantitative estimation of corrosion rate and the possible influence of rust mechanical properties around the steel rebar.

Conversely, the crack patterns obtained adequately reproduce those observed in the experiments (Figure 6). Firstly, a multiple diffuse crack scenario around the reinforcement bar is clearly shown. Once some localisation of discrete cracks appears, crack patterns are progressively moving away from those expected through axially symmetric analytical models. While vertical cracks do appear on the surface, as the corrosion process progresses cracks tend to localise on the horizontal plane between the reinforcement bars, as predicted by others [4]. In fact, with thicker concrete cover, early vertical cracks do not even appear on the top surface [23].

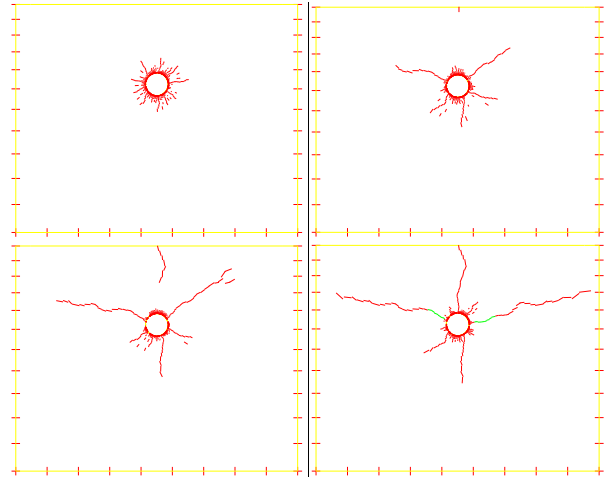


Figure 6: Crack pattern in slab specimen L1 (in green, consolidated cracks with width $> 0.1\text{mm}$).

3.3 Application case: upper slab in bridge deck

As a practical application of the previous model, a bridge deck upper slab exposed to chloride attack is analysed. A 2D finite element mesh is extracted from the actual bridge. Service life prediction is fully dependent on two basic variables not usually precisely known, the threshold chloride concentration and the corrosion rate. Then, major conclusions are referred to the achieved cracking pattern, which matches experimental results in accelerated corrosion tests (e.g. [27]). In Figure 7, cracks with width greater

than 0.1 mm are shown in green. In fact, a maximum width around 0.25 mm is reached in the last figure.

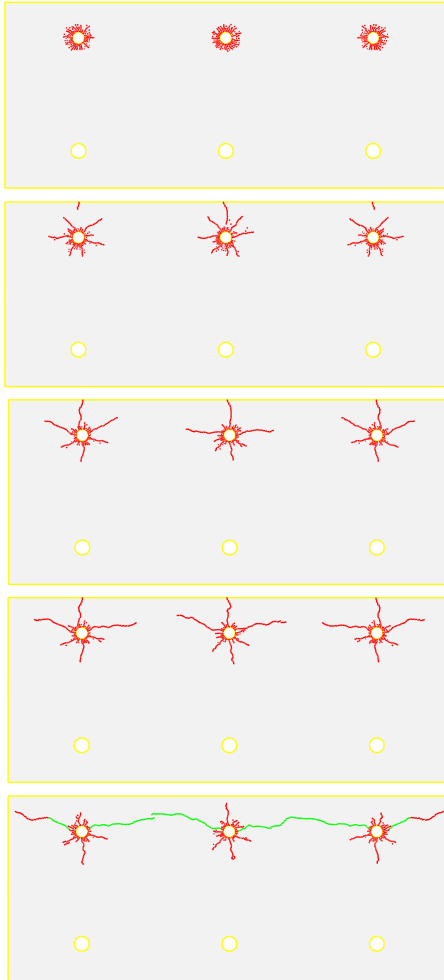


Figure 7: Upper slab in bridge deck. Sequential crack patterns due to rebar corrosion ($\Delta = 16 \mu\text{m}$, $32 \mu\text{m}$, $48 \mu\text{m}$, $64 \mu\text{m}$ and $80 \mu\text{m}$, respectively).

4 CONCLUSIONS

This work deals jointly with the two phases widely adopted in the literature concerning cover cracking of concrete due to rebar corrosion induced by chloride penetration: the initiation stage and the propagation stage. While in others these phases have been traditionally analysed separately, in this paper the models for both phases are incorporated in the same finite element program. Such models are chained, though not explicitly coupled, as a first step towards their future full integration.

Concerning the initiation stage, a comprehensive model is presented, focused on

the interdependence between chloride and moisture flows, with variable diffusion coefficients pending on temperature, humidity, and equivalent hydration time. Though electrostatic interaction among ions was neglected, some experimental results can be reproduced quite accurately. In addition, complex geometries, with explicit cracks included, can be simulated.

Concerning the propagation stage, an embedded cohesive crack finite element is proposed to model cover cracking. Time to surface cracking can be predicted, though it is necessary to make some assumptions about the consideration of an especially porous zone around the steel-concrete interface and the accommodation of corrosion products within the open cracks generated in the process. Moreover, the rust mechanical properties need further analysis. In addition, the crack patterns obtained agree well with experiments. As an example, crack patterns obtained by the application of the model to actual bridges match expectations.

ACKNOWLEDGEMENTS

The authors gratefully acknowledge the financial support for the research provided by the Spanish Ministerio de Ciencia e Innovación under grants IPT-42000-2010-31, DPI2011-24876 and BIA2010-18864.

REFERENCES

- [1] Kirkpatrick, T.J.; Weyers R.E.; Anderson-Cook, C.M. and Sprinkle, M., 2002. Probabilistic model for the chloride-induced corrosion service life of bridge decks. *Cement Concrete Res.*, **32**: 1943-1960.
- [2] Tuutti, K., 1982. Corrosion of steel in concrete. *Stockholm: Swedish Cement and Concrete Research Institute*.
- [3] Martín-Pérez, B.; Pantazopoulou, S.J. and Thomas, M.D.A., 2001. Numerical solution of mass transport equations in concrete structures. *Comput. Struct.*, **79**: 1251-1264.
- [4] Chen, D. 2006. Computational framework for durability assessment of reinforced

- concrete structures under coupled deterioration processes. *Ph.D. dissertation, Vanderbilt University, Nashville, Tennessee.*
- [5] Johannesson, B.F., 1997. Nonlinear transient phenomena in porous media with special regard to concrete and durability. *Adv. Cem. Based Mater.*, **6**: 71-75.
- [6] Samson, E.; Marchand, J.; Snyder, K.A. and Beaudoin, J.J., 2005. Modeling ion and fluid transport in unsaturated cement systems in isothermal conditions. *Cem. Concrete Res.*, **35**: 141-153.
- [7] Saetta, A.V.; Scotta, R.V. and Vitaliani, R.V., 1993. Analysis of chloride diffusion into partially saturated concrete. *ACI Mater. J.*, V. 90, No. 5.
- [8] Liu, Y. and Weyers, R., 1998. Modeling the time-to-corrosion cracking in chloride contaminated reinforced concrete structures. *ACI Mater. J.*, V. 95: No. 6: 675-681.
- [9] Bhargava, K. and Ghosh, A.K., 2003. Analytical model of corrosion-induced cracking of concrete considering the stiffness of reinforcement. *Struct. Eng. Mech.*, **16**: 749-769.
- [10] Molina, F.J.; Alonso, C. and Andrade, C., 1993. Cover cracking as a function of rebar corrosion: Part 2- Numerical model. *Mater. Struct.*, **26**: 532-548.
- [11] Bažant, Z. P. and Planas, J., 1998. Fracture and Size Effect in Concrete and Other Quasibrittle Materials. *CRC Press New York.*
- [12] Sancho, J.M.; Planas, J.; Gálvez, J.C.; Reyes, E. and Cendón, D.A., 2006. An embedded crack model for finite element analysis of mixed mode fracture of concrete. *Fatigue Fract. Engng. Mater. Struct.*, **29**, 1056-1065.
- [13] Sancho, J.M.; Planas, J.; Cendón, D.A.; Reyes, E. and Gálvez, J.C. 2007. An embedded crack model for finite element analysis of concrete fracture. *Eng. Fract. Mech.*, **74**: 75-86.
- [14] Taylor, R.L., 2005. FEAP- A Finite Element Analysis Program. Version 7.5 Programmer Manual.
- [15] Guzmán, S.; Gálvez, J.C. and Sancho, J.M., 2011. Cover cracking of reinforced concrete due to rebar corrosion induced by chloride penetration. *Cem. Concrete Res.*, **41**: 893-902.
- [16] Sergi, G.; Yu, S.W. and Page, C.L., 1992. Diffusion of chloride and hydroxyl ions in cementitious materials exposed to a saline environment. *Concrete Res.*, **44**: 63-69.
- [17] Wang, Y.; Li, L. and Page, C.L., 2005. Modelling of chloride ingress into concrete from a saline environment. *Build. Environ.*, Vol. 40, No.12, 1573-1582.
- [18] Morinaga, S. 1988. Prediction of service lives of reinforced concrete buildings based on rate of corrosion of reinforcement steel. *Special Report of Institute of Technology Shimizu Corporation, 23. Japan.*
- [19] Andrade, C.; Alonso, C. and Molina, F.J., 1993. Cover cracking as a function of bar corrosion: part 1- Experimental test. *Mater. Struct.*, **26**: 453-464.
- [20] Pantazopoulou, S.J. and Papoulia, K.D., 2001. Modeling cover-cracking due to reinforcement corrosion in RC structures. *J. Eng. Mech.*, Vol. 127, No. 4.
- [21] Bhargava, K.; Ghosh, A.K.; Mori, Y. and Ramanujam, S., 2006. Analytical model for time to cover cracking in RC structures due to rebar corrosion. *Nucl. Eng. Des.*, **236**: 1123-1139.
- [22] Chernin, L.; Val, D.V. and Volkh, K.Y., 2010. Analytical modelling of concrete cover cracking caused by corrosion of reinforcement. *Mater. Struct.*, Vol. 43, No. 4: 543-556.
- [23] Guzmán, S.; Gálvez, J.C. and Sancho, J.M., 2012. Modelling of corrosion-induced cover cracking in reinforced concrete by an embedded cohesive crack finite element. *Eng. Fract. Mech.*, **93**: 92-107.
- [24] Borja, R.I., 2000. A finite element model for strain localization analysis of strongly discontinuous fields based on standard Galerkin approximation. *Comput. Method. Appl. M.*, **190**:1529-49.
- [25] Liu, Y., 1996. Modeling the Time-to-Corrosion Cracking of the Cover Concrete in Chloride Contaminated Reinforced

Concrete Structures. *Ph.D. dissertation, Virginia Polytechnic Institute and State University, Blacksburg, Va.*

- [26]El Maaddawy, T. and Soudki, K., 2007. A model for prediction of time from corrosion initiation to corrosion cracking. *Cement Concrete Comp.*, **29**: 168-175.
- [27]Mullard, J.A. and Stewart, M.G., 2011. Corrosion-Induced cover cracking: new test data and predictive models. *ACI Struct. J.*, V. 108, No.1.